LAWRENCE
LIVERMORE
NATIONAL
LABORATORY

LLNL-JRNL-416496

Making Relativistic Positrons Using Ultra-Intense Short Pulse Lasers

H. Chen, S. Wilks, J. Bonlie, C. Chen, S. Chen, K. Cone, L. Elberson, G. Gregori, E. Liang, D. Price, R. Van Maren, D. D. Meyerhofer, J. Mithen, C. V. Murphy, J. Myatt, M. Schneider, R. Shepherd, D. Stafford, R. Tommasini, P. Beiersdorfer

September 2, 2009

Physics of Plasmas

Disclaimer

, , , , , , , , , , , , , , , , ,

Making Relativistic Positrons Using Ultra-Intense Short Pulse Lasers

Hui Chen[a], S. C. Wilks[a], J. D. Bonlie[a], C. D. Chen[a], S. N. Chen[a], K. Cone[a], L. Elberson[a], G. Gregori[b], E. P. Liang[c], D. F. Price[a], R. van Maren[a], D. D. Meyerhofer[d], J. Mithen[b], C. V. Murphy[b], J. Myatt[d], M. B. Schneider[a], R. Shepherd[a], D. Stafford[a], R. Tommasini[a], P. Beiersdorfer[a]

[a] *Lawrence Livermore National Laboratory, Livermore, California 94550, USA*
[b] *Clarendon Laboratory, University of Oxford, OX1 3PU, UK*
[c] *Rice University, Houston, TX 77005, USA*
[d] *University of Rochester, Rochester, NY 14623, USA*

Abstract

This paper describes a new positron source produced using ultra-intense short pulse lasers. Although it has been studied in theory since as early as the 1970s, the use of lasers as a valuable new positron source was not demonstrated experimentally until recent years, when the petawatt-class short pulse lasers were developed[1, 2]. In 2008 and 2009, in a series of experiments performed at Lawrence Livermore National Laboratory, a large number of positrons were observed after shooting a millimeter thick solid gold target. Up to 2×10^{10} positrons per steradian ejected out the back of ~mm thick gold targets were detected. The targets were illuminated with short (~1 ps) ultra-intense ($\sim1\times10^{20}$ W/cm^2) laser pulses [3]. These positrons are produced predominantly by the Bethe-Heitler process, and have an effective temperature of 2 – 4 MeV, with the distribution peaking at 4 – 7 MeV. The angular distribution of the positrons is anisotropic. For a wide range of applications, this new laser based positron source with its unique characteristics may complements the existing sources using radioactive isotopes and accelerators.

Key words: Positrons, Short pulse lasers, 52.38.-r, 52.38.Ph, 52.59.-f

1. Introduction

Since the invention of the chirped pulse amplification technique [4] by Strickland and Mourou at the University of Rochester in the mid 1980s, increasing amounts of laser energy have been compressed into smaller and smaller pulse lengths, yielding higher peak power and intensity. Peak laser intensities of about 10^{21} Wcm^{-2} are now readily achievable. Succeedingly higher intensities open up multiple new areas of physics, as illustrated in Fig. 1 [5], including electron-positron pair creation by the laser pulse.

Email address: chen33@llnl.gov (Hui Chen)

When an ultraintense laser beam irradiates a flat solid target, electrons in the target are accelerated to relativistic velocities by the strong electric field of the laser. The electrons quivering in the electric field of the laser focus region result in an energy given by $E = m_e c^2[1 + (eE_0/m_e\omega c)^2]^{1/2}$, where E_0 is the amplitude of the laser electric field, ω the laser frequency, e the electron charge, m_e the electron rest mass, and c being the velocity of light. For a laser with intensity of about 10^{20} Wcm^{-2}, a characteristic energy of the hot electrons excited in a solid target is about 4 MeV, which is sufficient to create electron-positron pairs when interacting with nuclei. In contrast, the direct process of pair creation by an ultraintense laser is to create pairs by the vacuum polarization caused by the strong electric field of these lasers. The threshold laser intensity for the direct process (which is also known as the Schwinger limit) is about 10^{28}Wcm^{-2}, which is beyond the capability of current laser technology, but has been observed in intense laser interactions with a 50 GeV electron beam [6].

There are two primary processes that create positrons through hot electrons. One is the Trident process [7], where electrons interact directly with nuclei and produce pairs. In the Bethe-Heitler (B-H) process [7], fast electrons make high energy bremsstrahlung photons that, in turn, interact with nuclei to produce electron-positron pairs.

Since first theorized in 1973 [8], the use of ultra-intense lasers to generate positrons has been studied in great detail through theory and modeling [9, 10, 11, 12, 13, 14, 15]. It has been predicted that for thick high-Z targets, positron generation by the Bethe-Heitler process [7] dominates over that from the Trident process [10, 13]. For thin targets (less than 30 microns for solid gold) the reverse is expected [11].

Laser produced MeV positrons open the door to multiple new avenues of antimatter research, including an understanding of the physics underlying astrophysical phenomena such as black holes and gamma ray bursts [16, 17], basic pair plasma physics [18, 19], positronium production and positronium Bose-Einstein condensates [20, 21, 22, 23]. These research areas often require large numbers of positrons, which are difficult to supply. An additional constraint is that the positrons annihilate quickly (on a nanosecond timescale) when brought into contact with matter. The use of short, ultra-intense, laser pulses represents a promising new approach to produce a large numbers of positrons, at high densities and on timescales much shorter than the annihilation time. As explained below, further increases in laser positron production are anticipated given technological increases in the available energy, intensity and repetition rate of short-pulse laser systems.

The next section describes the basic theory of laser-solid interaction, electron acceleration and pair creation. Section 3 discusses the experimental setup. Section 4 details positron detection mechanisms. Sections 5, 6 and 7 characterize different aspects of the laser-produced positrons seen in the data. The last section discusses future work.

2. Basic theory and modeling of laser electron acceleration and pair creation

When an intense laser interacts with a solid target, the laser energy is coupled to free electrons in a coronal plasma that is generated via the laser prepulse interacting with the solid near the critical plasma density. Extensive work has been done in this area [24, 25, 26]. Simplified electron acceleration mechanisms occur in three regimes according to the coronal plasma density. Near the critical plasma density ($n_e > 10^{21}$cm^{-3}), the majority of the absorbed laser energy goes into creating energetic electrons due to the ponderomotive potential. The hot electron temperature can be estimated using the ponderomotive scaling [27]

$T_{hot} \approx 0.511[(1 + I_{18}^2/1.37)^{1/2} - 1]\ (MeV)$

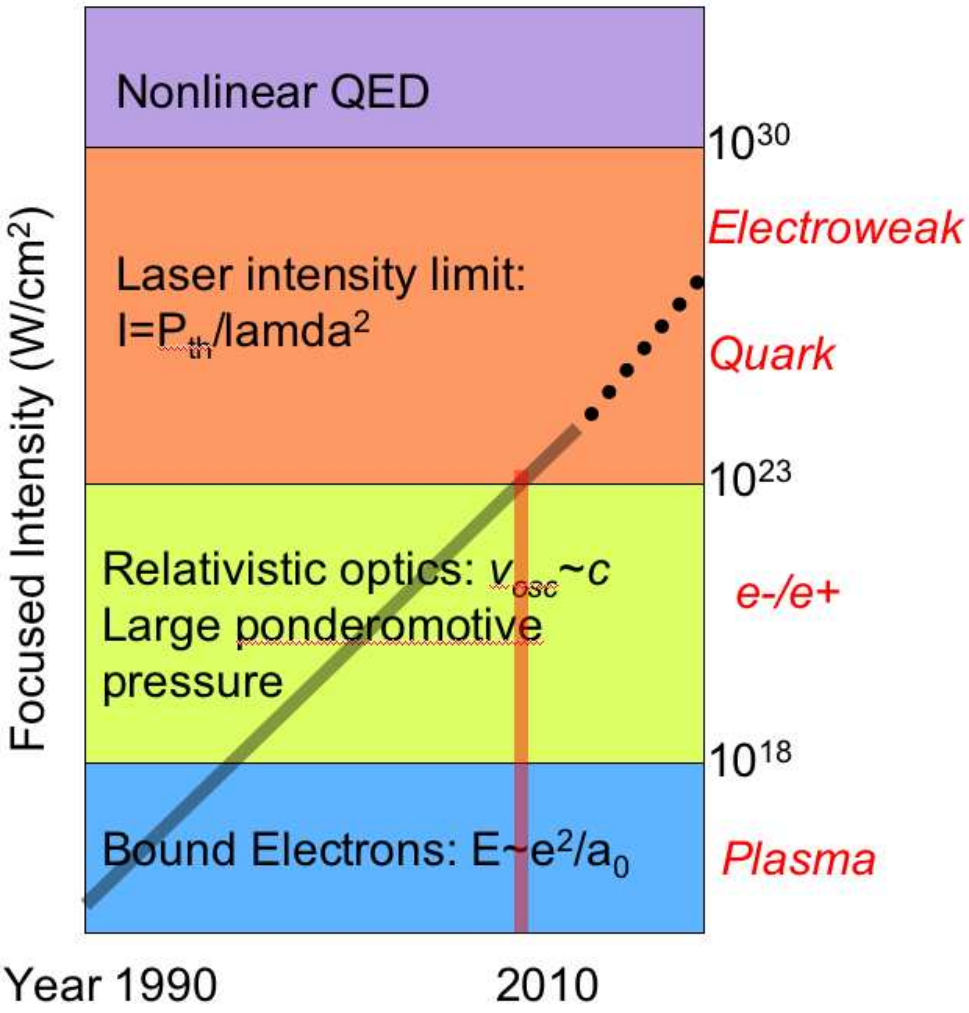

Figure 1: The peak intensity of short pulse lasers reached in the last 2 decades. Selected physics topics are highlighted for the related laser intensity region (courtesy of Bill Kruer [5]).

When the plasma density is less than critical and the density gradient (i.e. scale length) is long in the front of the solid target, another electron acceleration mechanism, the inverse free-electron laser mechanism becomes important. Computer simulations by Pukhov et al. (1999) [28] showed that the resulting hot electron temperature scaling for this mechanism is about three times higher than that from ponderomotive scaling,

$T_{hot} \approx 1.5(I/I_{18})^{1/2}$ (MeV)

The third electron acceleration mechanism that occurs when a long (few millimeters), low density (n_e <10^{18}cm^{-3}) plasma is present in front of the target. Known as self-phase modulated wakefield acceleration, this is related to the laser wake field accelerator idea that has been shown to drive mono-energetic bunches of electrons up to GeV energies[29]. This requires a finely tuned constant density over mm distances, matched with the laser energy and pulse lengths used to achieve a well-defined bunch energy. For an inhomogeneous low density pre-plasma created by a pre-pulse, there will be a continuum of electron energies ranging from a few keV to hundreds of MeV [3]. Self-phase modulated wakefield acceleration works by longitudinally (along the beam propagation direction) bunching the electrons into small bunches, the size of roughly a plasma wavelength creating a longitudinal oscillating electric field, consisting of both an accelerating and de-accelerating phase. Electrons trapped in the accelerating portion of the wave will be accelerated to some energy, depending on their relation to the phase of the wave, and how far they travel, before leaving the wave. In this way, a continuum of energies is obtained. Although the number of accelerated electrons by this method is low relative to the previous two mechanisms, the energy of individual electrons can be much higher, so its contribution to pair production cannot be neglected.

For maximum positron production, the key is to maximize the number of super hot (> 1 MeV) electrons produced from the laser-target interaction. Experimentally, the electron spectra mimic the ponderomotive scaling (eq. 1) for lower energy electrons, as shown in Fig. 2. For electron energies above about 5 MeV, 2 to 4 times higher electron temperatures are found than that from (eq. 1), suggesting inverse free electron acceleration (Eq. 2).

Once the hot electron distribution is known, the pair creation in solid targets can be calculated [9, 10, 11, 12, 13, 14, 15], and thus the positron yield vs laser intensity and target thickness can be estimated. Using analytical approaches, Myatt *et al*. [15] calculated the positron yield per kilojoule of hot electrons, as shown in Fig. 3, for various laser intensities, assuming the hot electrons were ponderomotively driven as described in Eq. 1.

The complexity of laser solid interaction is very challenging to simulate using just one model, and to do this correctly requires including the electrons from all three acceleration mechanisms. This is extremely difficult to do analytically, due to the 3-D characteristics of a realistic, nonuniform laser beam, and multiple timescales (sub femtosecond to nano second), and the uncertainty of the plasma parameters giving rise to such highly non-linear interactions. One must resort to modeling to estimate the number and energies of positrons produced in a particular experiment. One can first estimate the underdense plasma scale-length using a 3-D radiation-hydrodynamics code such as HYDRA [30] and then use a PIC (Particle-In-Cell) code, such as LSP or PSC (both 3-D models), to estimate the number and energy distribution of the hot electrons produced from the laser-plasma interaction. LSP is a simulation tool that runs macroparticles for both the solid target and the electrons. It generates the correct number of positrons by using cross sections generated by Monte Carlo electron-photon transport codes such as EGS and the Integrated Tiger Series code. LSP transports the electrons in self-consistent electric and magnetic fields. It will do a reasonable job at the transport of the relativistic electron beam through the solid gold. It self-consistently evolves the gold ions, electrons, positrons, and protons that may be present on

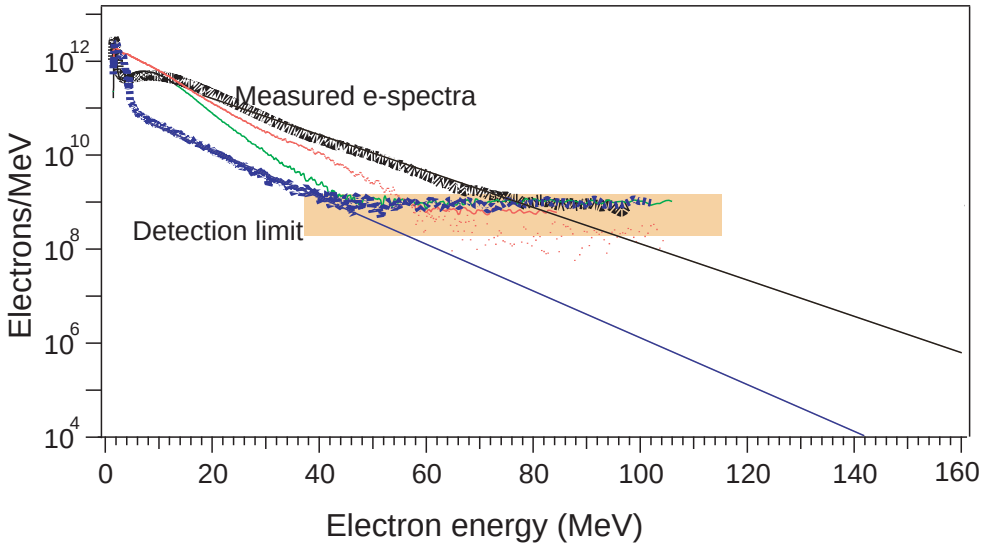

Figure 2: Hot electron energy spectra from various laser energies on the solid targets measured by the electron spectrometers (dots) and their extrapolations (lines).

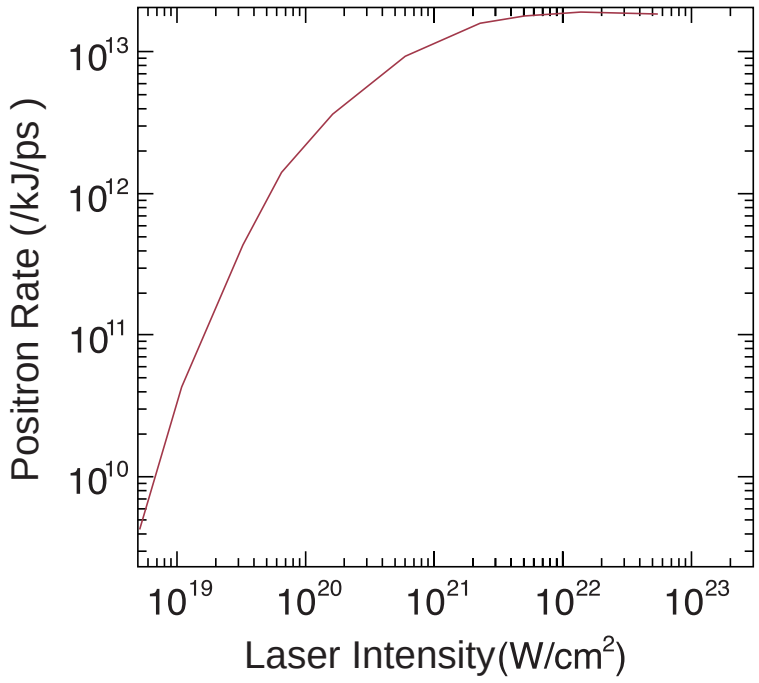

Figure 3: Electron-positron pair production rate per kJ of hot electrons as a function of laser intensity for the ponderomotive scaling[15] .

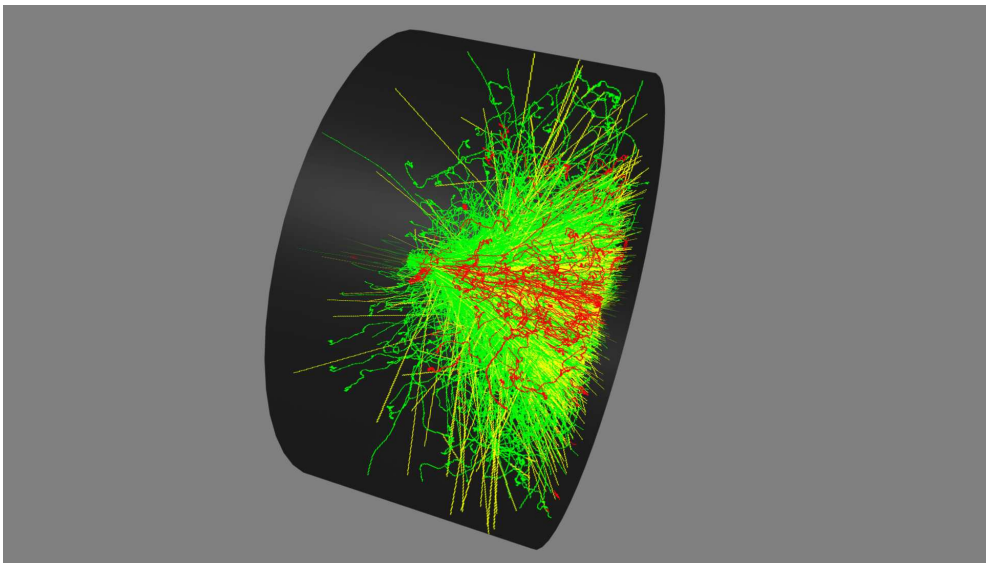

Figure 4: Simulated electron-photon-positron shower when 25 MeV electrons interact with a gold disk. The laser strikes from left, electrons (green) lose energy as they interact with gold nuclei and emit bremsstrahlung photons (yellow). Positrons (red) are produced when those photons interact with gold nuclei through B-H processes.

the rear and front surfaces of the gold foil [27]. For thicker targets (~ 1 mm) one can take the electron energy and number generated from PIC codes, then use a Monte Carlo electron-positron-photon transport code to estimate the number and energies of the positrons produced and then compare with experiment. An example is shown in Fig. 4, where a monoenergetic group of 25 MeV electrons was injected into solid gold using the EGSnrc code[43]. The entire spectrum of electrons with energies ranging from a few keV to 100 MeV is injected into the solid target. This method does not self-consistently describe electric and magnetic fields that influence the resulting positron spectrum when large numbers of positrons are produced.

All of the acceleration mechanisms mentioned above are only present when the laser is present. The source of the electrons that create the Bremsstrahlung, that in turn create the pairs exists only as long as the laser pulse is on. Since the energies of those particles of interest are relativistic (> 1 MeV) the time positrons are emitted is of order the laser pulse length as well.

3. Experimental setup

Earlier experiments on positrons using short pulse lasers were performed by Burke *et al*. [6] at Stanford linear accelerator, by Cowan *et al*. [1] on solid target using the Nova peta-watt laser [38], and by Gahn *et al*. on a gas jet target using a tabletop laser [2]. These two experiments demonstrated the ability of intense short laser pulses to create positrons in laser-solid interactions, although the numbers of positrons observed from these experiments were small ($<10^3$).

Positron generation experiments were carried out at the Titan laser at the Jupiter laser facility [37] at Lawrence Livermore National Laboratory. The pulse-length of the short pulse laser (1054 nm, *s*-polarized) was varied between 0.7 ps to 10 ps, and the laser energy was between 120 J to 250 J. The pre-pulse to main-pulse intensity contrast was less than (better than) 10^{-5}. An $f/3$

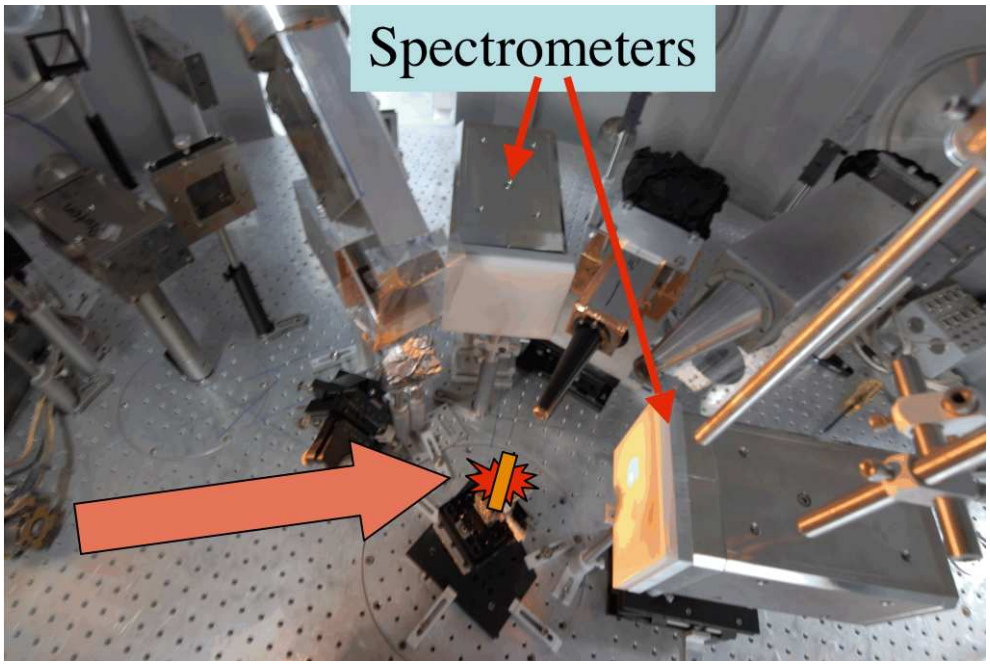

Figure 5: A picture of the experimental set up. The location of two spectrometers relative to the laser and target is marked.

off-axis parabola provides a full-width at half-maximum focal spot of about 8 microns that contains about 60% of the laser energy. The experimental setup is shown in Fig. 5. The short pulse was incident to the targets at an 18 degree angle. Two absolutely calibrated electron-positron spectrometers [32] observed the hot electrons and the positrons from the targets with energy coverage from 0.1 – 100 MeV and a resolution E/δE of 10 – 100, much improved from a previous positron spectrometer from which a hint of positron signal was observed [33]. The energy coverage and resolution are higher than achieved in the previous positron energy measurements [1, 2], where positrons were measured at only one [2] or several energy points [1].

The absolute calibration was made using electrons [34]. Because there is little difference ($\sim$ 2 – 3%) in positron and electron stopping in the detector materials [40], the electron calibration is applicable to the positrons. The solid angle for the rear spectrometer is 8.2×10^{-5} steradian and 4.5×10^{-5} steradian for the front spectrometer. The targets were disks of solid gold (Z=79), tantalum (Z=73), tin (Z=50), copper (Z=29), and aluminum (Z=13) with 6.4 mm diameter, and thicknesses ranging from 0.1 to 3.1 mm. Fig. 6 shows one of the targets.

4. Positron detection methods

Positrons can be detected directly or through their characteristic annihilation radiation. The harsh environment of intense short pulse laser experiments, where intense electromagnetic pulse (EMP) and radiation [31] are present, makes it difficult to use positron annihilation detection methods. Co-incident single gamma detectors would not function well due to the EMP and energetic photon fluxes.

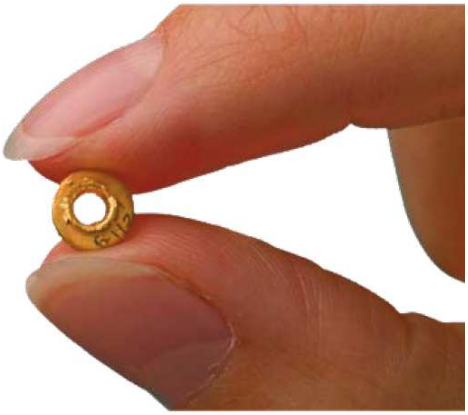

Figure 6: A picture of the gold target after it was shot. The target was 1 mm thick and 6.4 mm in diameter.

4.1. Direct positron measurement

Nuclear emulsion detectors were used in early laser-produced positron experiments by Cowan et al. [1]. While this method is almost single-particle counting, it is labor intensive. In the past few years, new, direct measurements of energetic electrons and positrons have been pursued, using either scintillating fibers [33], or image plates [33, 32]. Scintillators combined with photomultiplier tubes have been used by Gahn et al. in other laser-produced positron experiments[2]. The work reported here began using a scintillating fiber array coupled with fiber front CCDs, but later switched to image plates. The latter class of spectrometers are significantly more cost effective. They are physically compact, easy to use, and EMP insensitive.

Although a scintillating fiber array coupled to a CCD has the advantage of supporting remote data acquisition, without the need to break the detector vacuum, image plates have multiple advantages. Image plates allow much higher electron energy resolution than a scintillator array, due to their smaller pixel size. Image plates are insensitive to the EMPs from the ultra-intense laser-solid interactions, which present a harsh environment for CCD usage. Image plates are reusable and significantly more cost-effective. The use of image plates eliminates complex mechanical requirements, such as electrical vacuum feedthroughs and cooling systems, which are needed for use of CCDs on laser experiments.

Absolute calibrations of the fast electron response of image plates have been performed [34], allowing the absolute number of electrons or positrons to be inferred experimentally. The electron, proton and positron spectra are determined by dispersing an incoming stream of particles across the image plate detector. The principle of these charged particle spectrometers is illustrated in Fig. 7: a magnetic field generated from permanent magnets disperses charged particles according to their kinetic energy. In contrast to electromagnets, permanent magnets do not need an external power supply that could be affected by intense EMP in the short pulse laser environment.

Additional considerations in the spectrometer design include radiation shielding and signal filtering. Proper shielding is important to reduce the background in the detector caused by high-energy x rays and gamma rays generated in the laser chamber. Depending on the laser and target conditions, a single layer of high-Z material, such as tantalum or lead, may be sufficient for a laser intensities up to 10^{19} Wcm^{-2}, while for higher laser intensities, one may need a combination

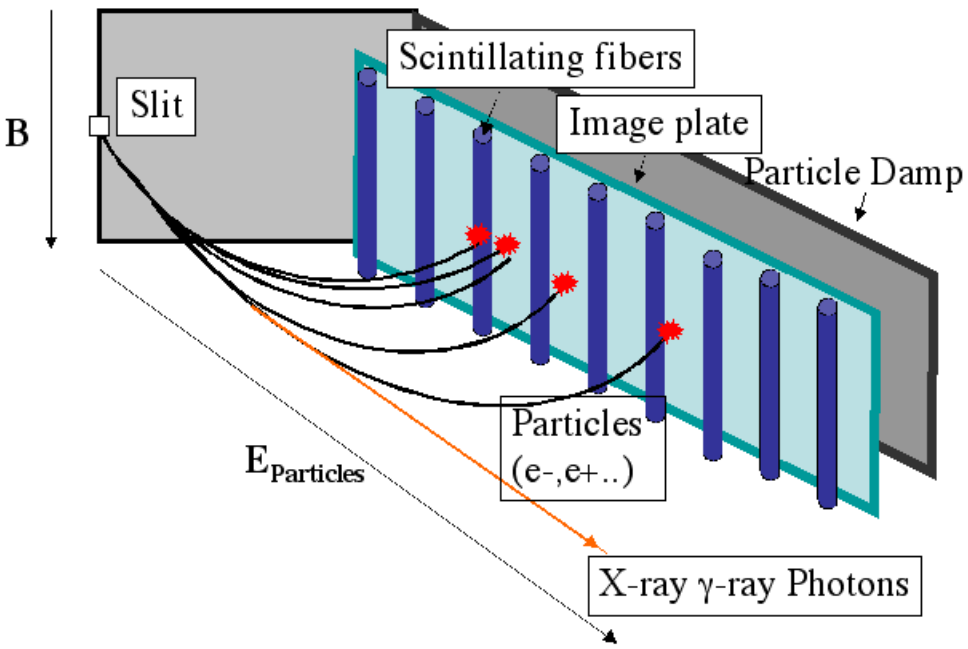

Figure 7: The principle of magnet electron/positron spectrometers used in our research.

of high-Z material (tantalum or lead) with medium-Z copper and aluminum to block the MeV photons and ions. In the work reported here, a considerable increase, by a factor of up to 100, in the signal-to-background ratio was achieved by employing the appropriate shielding for high intensity laser-solid interaction. Filters in front of the image plates can provide particle energy calibration (via stopping edges), and may provide simple discrimination among electrons and photons, or positrons, protons and other ions. For example, by adding a thin (20 μ m) layer of polypropylene, one can stop proton and ions at energy range less than 1 MeV.

4.2. Positron measurement through annihilation photons at 0.511 MeV

To obtain an energy spectrum of the photons from the target including the annihilation gamma radiation at about 0.5 MeV, a simple detection scheme is employed [35], using a stepwedge filter consisting of slabs of Pb of thicknesses of 0.5, 1.0, 2.0, 4.0, and 8.0 mm, as shown in Fig. 8(a). While the energy resolution of this setup is limited, it does not suffer from EMP and does not have pile-up issues, in contrast to electronic solid detectors such as Ge detectors or thick AmTec detectors. The combination of the step-wedge filter transmission and the image plate sensitivity provides a low-resolution energy spectrum. Under the assumption that the functional shape of the photon emission is known (such as one or two Maxwellian distributions), the x-ray spectrum can be retrieved by a best fit of the exposure values relative to the different filter thicknesses in the step-wedge filter. Assuming the emission to be dominated by bremsstrahlung, the conversion efficiency (CE) of laser energy into the energy of continuum emission in specific energy bands is calculated by integrating the derived spectra over the region of interest. The sensitivity of the imaging plate recording the step-wedge filter radiograph was simulated using the EGSnrc

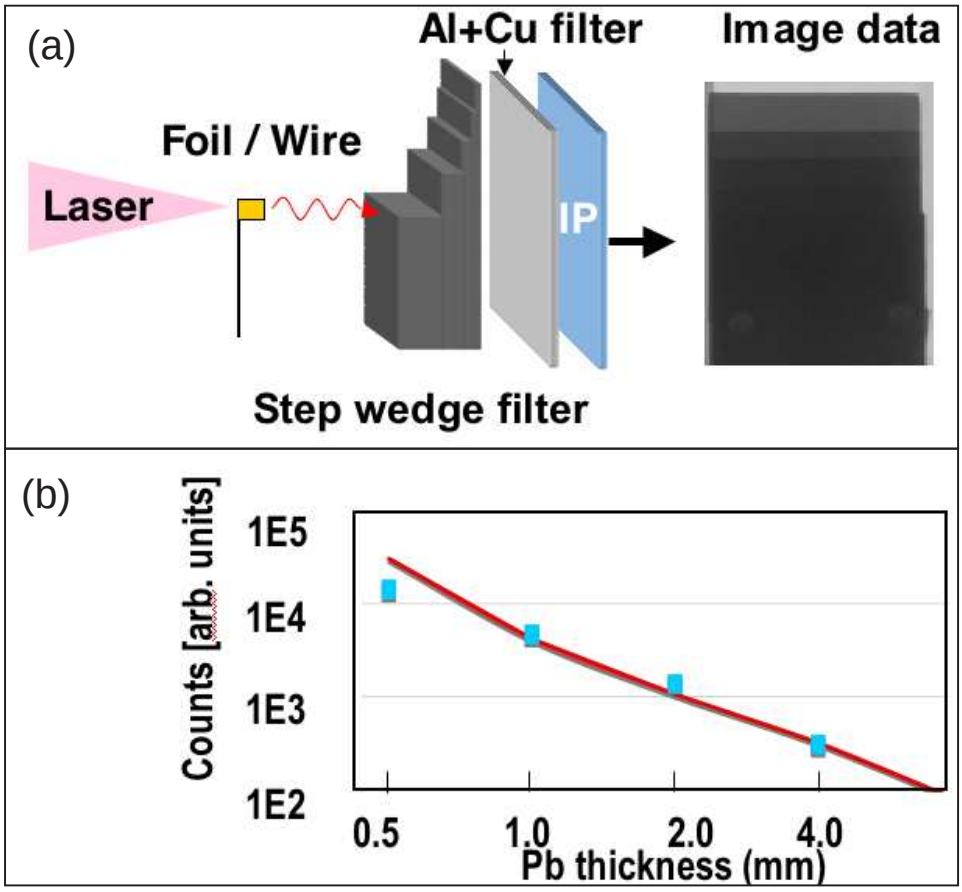

Figure 8: The principle of step filter spectrometer for high energy bremmstrahlung measurement.

Monte Carlo code. An example of the fitting procedure is shown in Fig. 8(b). If the 0.5 MeV annihilation radiation is substantial, one would expect to see an increase of photon flux in the region of annihilation energy.

5. Positron energy spectrum

Positron signals from short pulse irradiated Au and Ta targets are observed once the thickness exceeded 250 microns. Figure 9 shows the raw data image for a 1 mm Au target and the lineout through the signal and background.

The background seen in these data is mainly caused by high-energy photons passing through the housing of the spectrometer into the detector. Those photons may come directly from the target and from secondary radiation around the target chamber. The background evenly illuminates the detector beyond the slit and is easily subtracted from the signal, which comes only from the collimator and slit of the spectrometer. The signal was verified to be from positrons using methods such as: differentiating particles using mass stopping by adding plastic foils, and shooting

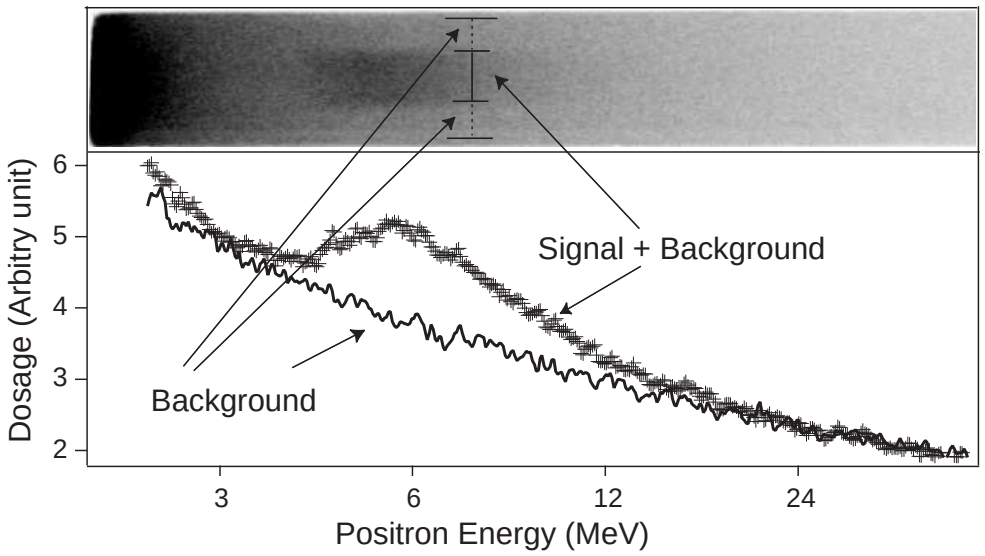

Figure 9: Raw positron data image and lineouts. This shot used a 2 ps pulse with 126 J of laser energy. The laser intensity was about 6 $\times 10^{19}$ W/cm^2. The target thickness was 1 mm.

lower-Z targets (including Al, Cu, and Sn) with the same laser conditions as for the Au targets. The spectra from these targets are shown in Fig. 10. While the hot electron production for the lower-Z targets was similar to that from Au, there was no positron signal above the background. The absence of signal was consistent with the Z^4 scaling of the B-H positron yield, which implies more than an order of magnitude fewer positrons in the lower-Z targets [13]. For thinner (0.1 to 0.25 mm) Au targets, positrons were not observed above the background. This is because fewer pairs are produced from thinner targets [13] due to the reduced interaction range between photons and electrons with Au nuclei. Thinner targets have more high-energy photon yield [38], which contributes to a higher background and a higher positron detection threshold.

The yield of positrons was determined by scaling the positrons to the number of hot electrons that were detected. The electron spectrum from the front spectrometer is similar to that of the rear spectrometer. The detection limit is about 1×10^8/MeV/sr for the rear spectrometer and about 2×10^7/MeV/sr for the front spectrometer. The higher energy section (5 – 45 MeV) of the electron spectrum is more relevant to positron creation and had a temperature (derived from the slope of the energy spectrum) of 4.8±0.4 MeV and an electron number of about 7×10^{11}/sr. The positron numbers are about 1.6×10^{10}/sr from the rear spectrometer and 2×10^9/sr from the front spectrometer. The peaks of both positron spectra are at about 6 MeV, and the effective positron temperature is 2.8±0.3 MeV. This first experimental positron temperature measurement enabled the electron and positron temperatures to be compared: the measured positron temperature was found to be approximately half that of the effective electron temperature.

6. Positron angular distribution

A strong anisotropy in the angular positron emission was observed from the rear and front of the target. Fig. 11 shows the positron spectra from both the front and rear spectrometers for a

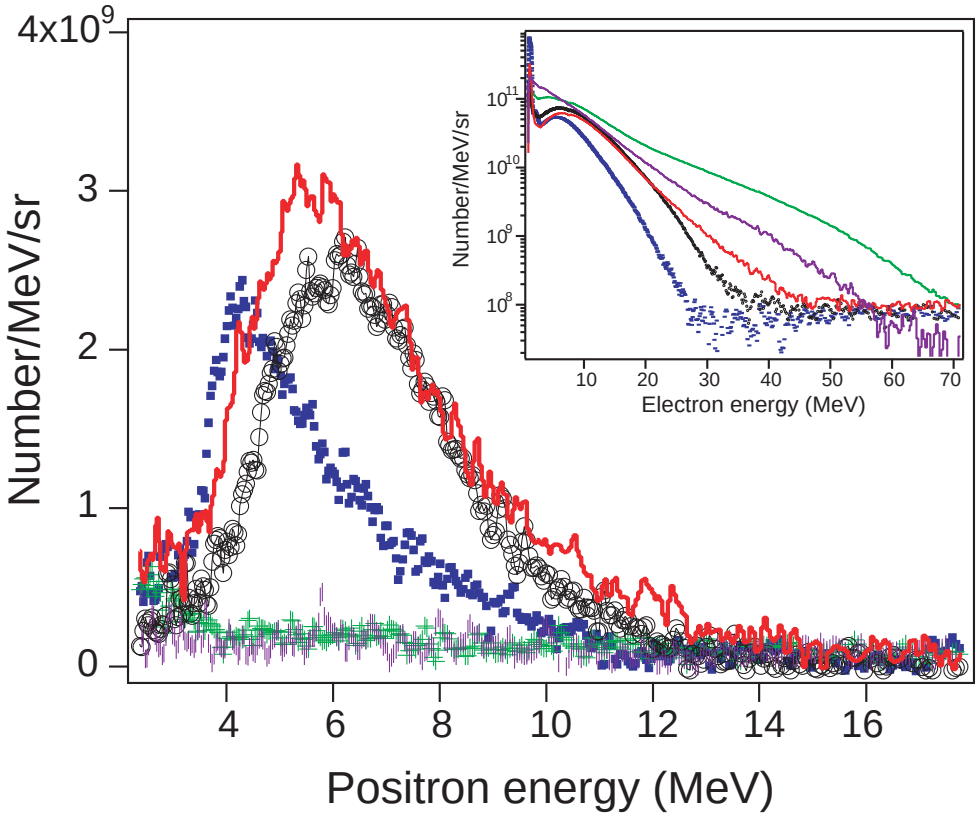

Figure 10: Positron spectra of targets of Au (three upper traces), Sn (green) and Cu (purple) from experiments - no positrons were detected for Cu and Sn targets. The inset are the electron spectra for the same shots (same color scheme).

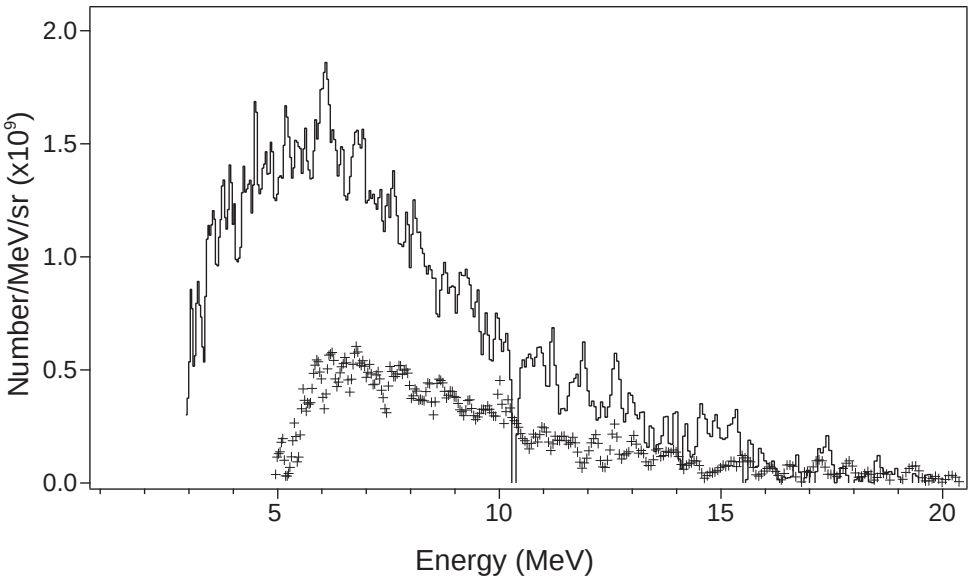

Figure 11: Positron spectra from back (upper trace) and front (lower trace) of the target.

126 J, 2 ps short-pulse shot. It was found that the number of positrons ejected near the normal to the rear of the target is more than 10 times the number more obliquely observed from the front of the target on a given shot. This is the first observation of an anisotropic distribution of the laser-generated positrons.

The positron distribution around the target was further measured, and as shown in Fig. 12, the peak of the positron numbers appears near the laser axis, at the back of the target. This feature may be significant if a future laboratory astrophysical experiment is designed to simulate the astrophysical electron positron jets [15].

While the inferred hot electron numbers for the Nova petawatt experiment [1] were similar to that measured in this experiment, more than two orders of magnitude more positrons were observed from the rear of the target in the present experiment than in the Nova petawatt experiment. In the Nova experiment the positrons were measured at the rear of the target, 30 degrees from the laser axis [1]. The difference may be due to the preformed plasma conditions, target thickness (~1 mm on Titan versus 0.125 mm on Nova PW), and possibly a sub-optimal observation angle used on Nova.

7. Data Modeling

Calculations using the measured hot electron temperature with the given target parameters show that the MeV x-ray bremsstrahlung photons (BH process) dominate the positron production within thick targets [3]. The ratio of positrons generated by the BH versus Trident processes is $N_{BH}/N_{Trident}$ ~ 400 for 1 mm thick Au (compared to about 4 for a 0.1 mm Au target.) The positron temperature can be estimated from a simple formula $dN_{e+}/dE_{e+} = \int_E f(E)\sigma_{BH}(E,E_{e+})dE$, where $f(E)$ is the bremsstrahlung photon energy distribution, and σ_{BH} is the positron creation differential cross section [7]. Approximating the bremsstrahlung temperature to be that of the

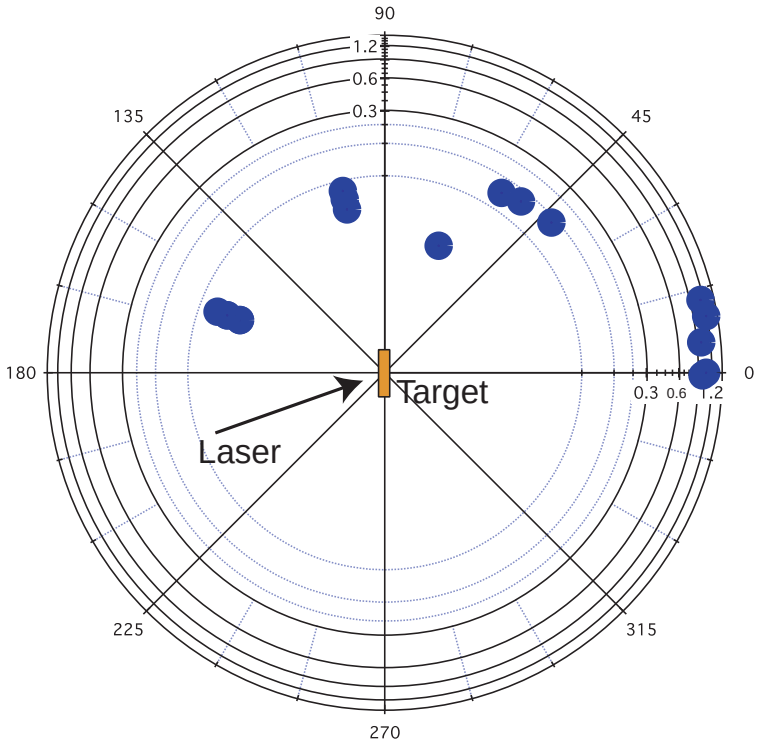

Figure 12: Polar plot of positron numbers (solid circles) at various positions around the target. The peak appears at the back of the target near laser axis.

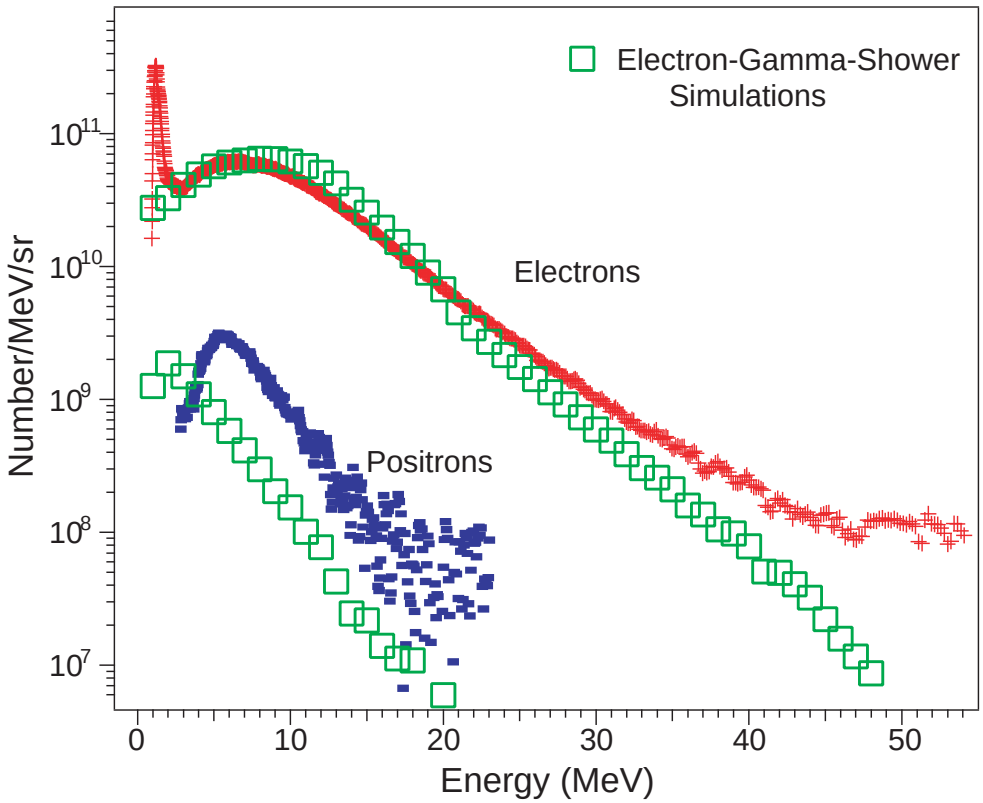

Figure 13: Energy spectra of electrons (red crosses) and positrons (blue solid squares) from experiments and EGS modeling (empty squares).

measured hot electrons, an effective temperature for the positrons of about half that of the electrons is obtained, as shown in Fig. 13. This is consistent with the experimental data.

The positron spectrum obtained from the above calculation is for all positrons generated inside the target. To model the emergent positron spectrum (that measured by the spectrometer), one has to fold in the positron transport inside the target. This was accomplished by a Monte Carlo code EGSnrc [43]. This code includes only BH pair production and is well suited for our thick target experiments. In addition to calculating the positron generation, it self-consistently treats the attenuation effects of the electrons, photons, and positrons as they propagate through a cold solid target. The measured hot electron temperature shown in Fig. 13 is used as the starting distribution of hot electrons. The positron spectra outside the target were modeled at the same angular positions relative to the target as in the experiment. The simulated positron spectra agree not only with the positron temperature (slope of the spectrum) seen in the experiment, but also with the relative positron number. It is noted that the peak of positrons from the simulation is at about 2 MeV (as in a previous prediction [13]), rather than at the measured ~6 MeV. This discrepancy may be due to the fact that neither the analytic formula nor EGS simulations include plasma effects. A sheath electric field is expected to accelerate the positrions leaving the target, similar to the target normal sheath acceleration field (typically of order of several MeV) for

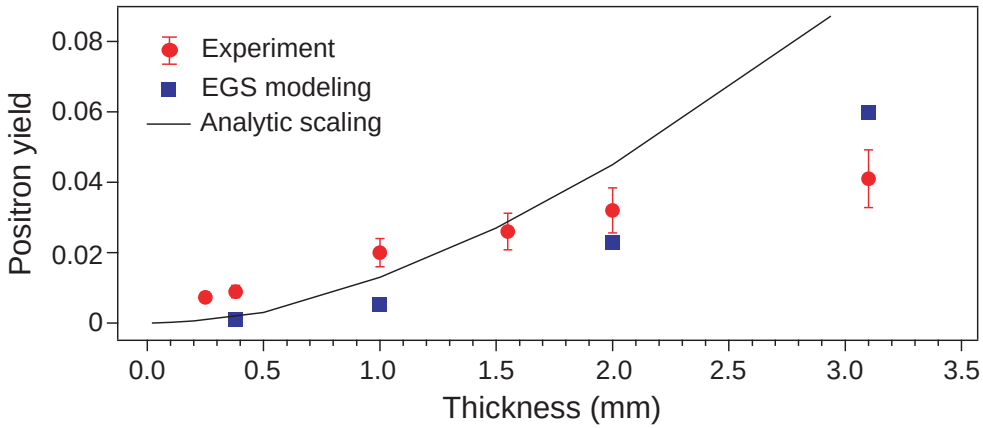

Figure 14: Positron yield per hot electron as a function of Au target thickness. The short-pulse duration was 0.7 ps for all data points. The laser intensities were from 1.5 – 1.8 $\times 10^{20}$ W/cm^2, hot electron temperature from 5.5 – 7 MeV.

protons [27, 45]. This is supported by the fact that protons with energies of 1 – 4 MeV were observed at the rear of the target for the shot shown in Fig. 13 and the same sheath field that accelerates the protons would influence the front and rear positron spectra.

The yield of positrons increases as a function of hot electron temperature for a given target thickness, as theoretically predicted[13]. The yield of positrons also increases as a function of target thickness, as shown Fig. 14. Theoretically, the increase of positron yield with target thickness has been shown for thinner targets by Nakashima and Takabe [13]. For a thick target (2 mm lead), Gahn *et al*. [44] calculated that for an electron kinetic energy above 5 – 15 MeV, the positron yield is between 5×10^{-3} and 4×10^{-2}, comparable to our measured yield of about 2×10^{-2}. Figure 14 shows the results from the analytical model and simulation using EGS for these experimental conditions. In the analytic model, the yield was estimated using the BH pair creation process combined with positron and electron attenuation inside the target, indicating that the positron yield per hot electron detected increases as target thickness, until the target thickness is greater than about 5 – 6 mm. Although there is a general qualitative agreement between theory/modeling and experiments, both the analytic model and the EGS simulation underestimate the positron yield for thickness less than 1 mm. This difference may again be due to differences in angular distributions of positrons versus electrons and complex plasma effects, such as electron/positron transport and the electromagnetic field, lacking in the theory and EGS modeling.

8. Future work

The positron data corresponds to 2×10^{10} observed positrons/sr for about 120 J laser energy for 1 mm target. From the EGS simulations, at least a factor of 10 more positrons are expected to be trapped inside the target. Given the bremsstrahlung photon and target interaction volume, which are determined from the simulation to be approximately 2×10^{-5} cm^3, the positron density in the target is estimated to be about 1×10^{16} positrons/cm^3, albeit in the presence of gold atoms at solid density. If all of the positrons are created in the order of ~ps, then the rate of positron

production is of the order of 2×10^{22}/s/sr. In the future, as high energy (100's of Joules), high repetition rate (>10 Hz) short pulse laser sources become available, the average positron production rate could approach 10^{10}/s/sr, which is comparable to existing positron sources [39].

There are plans to pursue the laser produced positron research further, using newly available petawatt class laser facilities. The OMEGA EP laser[46] recently started operation at Rochester University, and the Texas Petawatt laser, at the University of Texas (Austin) has completed construction. OMEGA EP has over an order of magnitude more short-pulse laser energy than the Titan laser. Since the number of positrons scales with energy, 10 times more positrons might be expected from a kJ class short pulse laser like OMEGA EP, and even higher numbers with more energetic lasers such as NIF-ARC [47]. It might even be possible to make, in the laboratory, miniature Gamma-ray bursts using the unique characteristics of laser produced electrons and positrons. These would not only be the first set of experiments that generate and characterize relativistic pair plasmas, but they might also help to realize many of the new, exciting applications mentioned above, including confirming the existence of a novel astrophysical mechanism theorized to be the cause of gamma ray bursts.

This work was performed under the auspices of the U.S. DOE by LLNL under Contract DE-AC52-07NA27344 and was funded by LDRD-08-LW-058. Additional support was provided from LLNL's Institute for Laser Science and Applications. Work performed by the University of Rochester was supported by the U.S. DOE Office of Inertial Confinement Fusion under No. DE-FC52-08NA28302, the University of Rochester, and the New York State Energy Research and Development Authority. Work performed by Rice University was supported by NSF AST-0406882 and the Rice Faculty Initiative Fund. The authors gratefully acknowledge support from the staff at Jupiter Laser Facility and Drs. Mark Eckart, Robert Cauble, William Goldstein and Don Correll, and discussions with Dr. Robert Heeter.

References

[1] T. E. Cowan *et al*., Laser Part. Beams **17**, 773 (1999).
[2] C. Gahn *et al*., Applied Physics Letters **77**, 2662 (2000).
[3] Chen, H., Wilks, S. C., et al., Phys. Rev. Lett. **102**, 105001 (2009)
[4] D. Strickland and G. Mourou, Opt. Commun. **56**, 219 (1985)
[5] Frontiers in High Energy Density Physics: The X-Games of Contemporary Science (National Academies Press, 2003)
[6] D. L. Burke *et al*., Phys. Rev. Lett. **79**, 1626 (1997)
[7] W. Heitler, The Quantum Theory of Radiation (Clarendon Press, Oxford, 1954)
[8] J. W. Shearer *et al*., Phys. Rev. A **8**, 1582 (1973).
[9] P. L. Shkolnikov *et al*., Appl. Phys. Lett. **71**, 3471 (1997).
[10] D. A. Gryaznykh Y. Z. Kandiev, and V. A. Lykov, JETP Lett. **67**, 257 (1998).
[11] E. P. Liang, S. C. Wilks, and M. Tabak, Phys. Rev. Lett. **81**, 4887 (1998).
[12] B. Shen and J. Meyer-ter-Vehn, Phys. Rev. E. **65**, 016405 (2001).
[13] K. Nakashima and H. Takabe, Phys. Plasmas **9**, 1505 (2002).
[14] V.I. Berezhiani, D.P. Garuchava and P.K. Shukla, Physics Letters A **360**, 624 (2007).
[15] J. Myatt *et al*., Phys. Rev. E,**79**, 066409 (2009).
[16] J. Wardle *et al*., Nature **395**, 457 (1998).
[17] P. Meszaros, Annal Review of Astronomy and Astrophysics **40**, 137 (2002).
[18] H. A. Weldon, Phys. Rev. Lett. **66**, 293, (1991).
[19] E. G. Blackman and G. B. Field, Phys. Rev. Lett. **71**, 3481, (1993).
[20] P. M. Platzman and A. P. Mills Jr. Phys. Rev. B. **49**, 454 (1994).
[21] A. P. Mills Jr., Nucl. Instrum. and Methods in Phys. Research Sec. B, **192**, 107, (2002)
[22] D. B. Cassidy and A. P. Mills, Jr. Phys. Stat. Sol. **4**, No. 10, 3419 (Willey Interscience, 2007).
[23] E. P. Liang and C. D. Dermer, Opt. Comm. **65**, 419 (1988).
[24] Kruer, W. L. The physics of laser plasma interactions (Addison-Wesley Publishing Co. 1988)

[25] Gibbon, P., Short Pulse Laser Interactions with Matter: An Introduction (World Scientific Publishing Company, 2005)
[26] R. Paul Drake, High-Energy-Density Physics: Fundamentals, Inertial Fusion, and Experimental Astrophysics (Springer, 2006)
[27] S. C. Wilks *et al.*, journalPhysics of Plasmas **volume8**, pages542 (year2001).
[28] Pukhov, A., Sheng, Z-M. and Meyer-ter-Vehn, J. Physics of Plasmas **6**, 2847 (1999)
[29] Leemans, W., and Esarey, E. Physics Today **62**, 33 (2009)
[30] Marinak, M., *et al*., Phys. Rev. Lett. **75**, 3677 (1995)
[31] C. Stoeckl, *et al*., Rev. Sci. Instrum. **77**, 10F506 (2006)
[32] H. Chen *et al*., Rev. Sci. Instrum. **79**, 10E533 (2008).
[33] H. Chen *et al*., Rev. Sci. Instrum. **77**, 10E703 (2006).
[34] H. Chen *et al*., Rev. Sci. Instrum. **79**, 033301 (2008).
[35] R. Tommasini, *et al*., Rev. Sci. Instrum. **79**, 10E901 (2008)
[36] C. D. Chen, *et al*., Rev. Sci. Instrum. ??? **79**, 10E901 (2008)
[37] http://jlf.llnl.gov
[38] S. P. Hatchett *et al*., Phys. Plasmas **7**, 2076 (2000).
[39] C. M. Surko and R. G. Greaves, Physics of Plasmas **11**, 2333 (2004).
[40] F. Rohrlich and B. C. Carlson, Phys. Rev. **93**, 38 (1954).
[41] S. C. Wilks *et al*., Phys. Rev. Lett. **69**, 1383 (1992).
[42] J. Krall et al., Phys. Rev. E **48**, 2157 (1993); N. E. Andreev et al., Physica Scripta **49**, 101 (1994); C. D. Decker and W. B. Mori, Phys. Rev. Lett. **72**, 490 (1994); E. Esarey et. al. Phys. Rev. Lett. **72**, 2887 (1994)
[43] I. Kawrakow and D. W. O. Rogers, National Research Council of Canada Report PIRS-701 (2006).
[44] C. Gahn *et al*., Physics of Plasmas **9**, 987 (2002).
[45] R. A. Snavely,*et al*., Phys. Rev. Lett. **85**, 2945 (2000)
[46] L. J. Waxer *et al*., Opt. Photonics News **16**, 30 (2005).
[47] M. H. Key, Phys. Plasmas **14**, 055502 (2007).